JREE: Vol. 11, No. 3, (Summer 2024) 42-51

Journal of Renewable Energy and Environment

Journal Homepage: www.jree.ir

Materials and Energy Research Center

MERC

Research Article

Optimization and Modeling of Process Parameters on Bio-Char Yield of Low- and High-density Sawdust for Solid Fuel

Oluwasanmi Iyiola Alonge [a]*, Olusola Ayodele Oloruntoba [b], Temitayo Samson Ogedengbe [c], Adedotun Michael Adedoja [d], Imisioluwa Adelere Akintola [e]

[a] Department of Mechanical Engineering, Faculty of Engineering, Elizade University, Ilara-mokin, Ondo State, P.O.BOX: 340271, Nigeria.
[b] Department of Automotive Engineering, Faculty of Engineering, Elizade University, Ilara-mokin, Ondo State, P.O.BOX: 340271, Nigeria.
[c] Department of Mechanical Engineering, Faculty of Engineering, Nile University of Nigeria, Abuja, P.O.BOX: 900001, Nigeria.
[d] Department of Mechanical Engineering, Faculty of Engineering, Redeemer's University, Ede, Osun State. P.O.BOX: 232101,Nigeria.
[e] Department of Chemical Sciences, Faculty of Science, Kings University, Odeomu, Osun State, P.O.BOX: 220104, Nigeria.

PAPER INFO

Paper history:
Received: 20 November 2023
Revised: 05 March 2024
Accepted: 23 June 2024

Keywords:
Biochar,
Optimization,
Carbonization,
Temperature,
Residence Time,
Particle Size

ABSTRACT

Biochar has garnered significant attention as a potential substitute due to its favorable adaptability and equivalent metallurgical characteristics to coal and coke. An investigation was conducted to maximize the production of biochar with enhanced characteristics by carbonizing low-density (LDS) and high-density sawdust (HDS). The study utilized the Response Surface Methodology to predict the combined impact of processing factors, namely temperature, particle size, and residence time, on the yield of biochar. The aim was to identify the ideal circumstances that would result in an enhanced biochar yield. The optimum values for the HDS were numerically predicted as a temperature of 498.24°C, a residence time of 21.16 minutes, and a particle size $0.6 \leq x \leq 0.8$ mm. Under these conditions, the predicted fixed carbon yield was 57.40%, and the corresponding percentage yield was 25.54%. The optimum values for LDS were numerically predicted as a temperature of 474.70°C, a residence time of 25 minutes, and a particle size $0.6 \leq x \leq 0.8$ mm. Under these conditions, the predicted fixed carbon yield was 51.26%, and the corresponding percentage yield was 30.60%. The optimized biochar for the two types of sawdust exhibited improved energy contents (30 MJ/kg for HDS and 26.24 MJ/kg for LDS) and chemical elements comparable to coal, indicating that the biochar will be suitable for power generation. The study also concluded that temperature has the most significant effect on the quality of biochar produced from both HDS and LDS.

https://doi.org/10.30501/jree.2024.425270.1735

1. INTRODUCTION[1]

An estimated 580 million terajoules of energy are consumed annually worldwide. This corresponds to 13.9 billion tons of oil equivalent (Mtoe), or 580 million trillion joules (*https://www.Theworldcounts.Com/*). In 2020, fossil fuels, nuclear energy, and renewable energy sources (primarily hydro, wind, and solar) comprised 83%, 12.6%, and 6.3% of global energy consumption, respectively. To achieve zero fossil fuel use by 2050, renewable energy output must increase by up to six or eight times, depending on whether energy consumption remains at the 2020 level or rises by 50% (Holechek et al., 2022). Current human development, driven by significant advancements in industrialization and modernization, has resulted in overconsumption of fossil fuels and severe environmental problems. The heavy reliance on fossil fuels in industrial processes has led to excessive emissions of exhaust gases (such as CO_2, SOx, and NOx), contributing to global warming and environmental degradation (Gnanasekaran et al., 2023; Zhou et al., 2023). Therefore, it is imperative to find effective, ecologically sound alternatives to ensure the sustained progress of both present and future generations. Transitioning to a sustainable low-carbon energy system would help countries address the issues caused by rapid population and economic growth, which result in high levels of carbon dioxide emissions (Adeboye et al., 2021). Like other developing countries, Nigeria faces numerous energy-related challenges, including environmental issues from fossil fuel exploration and exploitation, depletion of fossil fuel reserves, electricity shortages due to population growth, and inadequate government planning (Adeboye et al., 2021).

Among the available renewable energy sources—biomass, solar, wind, and hydropower—biomass is the most feasible option for conversion into biofuels. It is crucial to manage biomass waste cleanly. Biomass refers to any materials of animal, plant, or microbial origin. Plant-based biomass is especially valued for its availability and its capacity to reduce greenhouse gas emissions (Gnanasekaran et al., 2023).

Biomass energy constitutes a significant portion of the total energy supply in Eastern and Southern Africa, accounting for around 70% of the continent's total energy consumption.

*Corresponding Author's Email: *alongeoluwasanmi@gmail.com* (O. I. Alonge)
URL: https://www.jree.ir/article_199106.html

Please cite this article as: Alonge, O. I., Oloruntoba, O. A., Ogedengbe, T. S., Adedoja, A. M. and Akintola, I. A. (2024). Optimization and Modeling of Process Parameters on Bio-Char Yield of Low- and High-density Sawdust for Solid Fuel, *Journal of Renewable Energy and Environment (JREE)*, 11(3), 42-51. https://doi.org/10.30501/jree.2024.425270.1735.

Biomass fuels can not only address fuel shortages but also aid in waste management and the reduction of carbon dioxide emissions (Zhao et al., 2022). Additionally, biofuels can enhance energy independence and security, and create new economic opportunities in rural areas by stimulating demand for agricultural products and creating jobs in related industries (Rentizelas et al., 2009).

Wood, one of the oldest biomaterials, remains the most widely used natural resource (González et al., 2020). There are two types of wood: softwood and hardwood. Hardwood comes from plants that produce seeds with coverings (Osamah, 2006). Hardwood is categorized into three groups based on its moisture content at 15%: high-density hardwood (800-1120 kg/m³), medium-density hardwood (720-880 kg/m³), and low-density hardwood (400-720 kg/m³) (Alonge & Obayopo, 2023). Sawdust, a byproduct of woodwork processes such as sawing, planning, milling, drilling, and sanding, is readily available in large quantities and consists of both coarse and fine wood particles (Rominiyi et al., 2017).

Direct burning of solid biomass is the most straightforward and popular method for producing heat and energy from biomass resources (Álvarez-Bermúdez et al., 2023). However, burning solid biomass generates dangerous and toxic pollutants like nitrogen oxides (NOx), carbon monoxide (CO), and particulate matter (PM). Additionally, inorganic compounds in biomass fuel can cause problems related to ash, such as fouling, slagging, and corrosion, leading to reduced thermal efficiency and damage to combustion systems (Cai et al., 2018). The two primary methods for converting biomass in the context of a biorefinery are thermochemical and biochemical processes. These methods enable efficient biomass utilization for energy and recovery of value-added products. Biochemical processes are best for converting biomass to fuel alcohols, while thermochemical processes (combustion, gasification, pyrolysis, and liquefaction) are suitable for producing hydrocarbons and synthesized fuels (Alonge & Obayopo, 2023; Archer & Steinberger-Wilckens, 2018; Yang et al., 2019). Each process has inherent limitations that require technological improvements for efficient biomass conversion. Pyrolysis has gained significant attention over the past decade due to its advantageous operating conditions and diverse outputs, including biochar, bio-oil, and biogas. Pyrolysis is a thermal decomposition process where biomass is broken down in the presence of an inert medium. This medium prevents combustion, reduces the thermal stability of biomass at high temperatures, and minimizes secondary vapor-phase cracking reactions (Li et al., 2021).

Pyrolysis can be either rapid or slow. Fast pyrolysis, which aims to produce bio-oil, involves short solid/vapor residence times (1-2 seconds) and high heating rates (500 W/m² K). For producing a solid product (char), slow pyrolysis with longer residence times is preferable. Traditionally known as "charcoal," biochar has been used historically as a fuel source for industrial activities, cooking, and heating. This practice continues in many areas with limited access to alternative fuel sources (Lehmann & Joseph, 2015). Beyond its use as fuel, biochar can serve as a soil improver, activated carbon, and animal fodder additive.

Slow pyrolysis, also known as carbonization, occurs at lower temperatures (400-500°C), lower heating rates (5-20°C/s), and longer residence times (5-30 minutes) (Tripathi et al., 2016). This approach enhances char yield by minimizing secondary thermal cracking and the release of volatile components from biomass (Li et al., 2021). Both process parameters and feedstock characteristics influence the amount of biochar produced by slow pyrolysis. According to Tripathi et al. (2016), critical operational parameters during pyrolysis include temperature, pressure, reaction time, and particle size. Particle size directly affects the rate of heat transfer to the biomass core and the distance vapor travels through the char layer, leading to more secondary reactions and increased char production. Higher biochar yields are achieved at lower temperatures and longer residence times. Residence duration also impacts biochar quality and attributes by promoting pore development. High-quality biochar is characterized by high carbon content, large surface area, high porosity, functional groups, and stability (Tripathi et al., 2016).

This research study focuses on optimizing process parameters in the carbonization of low- and high-density sawdust in a fixed bed reactor for efficient biomass conversion and high-quality biochar production. The study aims to develop an effective strategy for operations planning, recycling, and waste management. Additionally, the study will establish the viability of obtaining optimal parameters by considering the interaction between various parameters.

2. METHOD

2.1. Materials and Experimental Analysis

Sawdust derived from *Ceiba pentandra*, a type of low-density wood, and *Nauclea diderrichii*, a type of high-density wood, was acquired from a Nigerian sawmill in the form of fine particles. Before characterization, the samples underwent a three-day sun-drying process until the moisture content reached the required amount of 10-16% for solid fuel, as specified by ASTMD2016-25 (Debdoubi et al., 2005). The desiccated specimens were separated into three distinct particle sizes (<0.6, $0.6 \leq x \leq 0.8$, $0.8 < x \leq 1$ mm) using an SV0005 electromagnetic sieve shaker. The particle sizes were achieved using sieve sizes of 600, 800, and 1000μm. Proximate and ultimate analysis of the samples were carried out using various methods, as shown in Table 1.

Table 1. Methods employed for proximate and ultimate analysis.

Property	Standard Method
Moisture Content (MC)	ASTM D2016-25
Volatile Matter (VM)	ASTM E872
Ash Content (AC)	ASTM D1102
Fixed Carbon (FC = 100-VM-AC-MC)	By difference
Carbon, Hydrogen and Nitrogen	ASTMD5373
Sulphur	ASTMD4239-11
Oxygen (N% + C% + S% + H% - 100)	By difference

The results of the characterization are presented in Table 2. No direct relationship was observed between moisture content and energy content. Moisture content is one of the main factors controlling solid biofuel quality. The moisture content of biomass significantly impacts both the internal temperature changes of the biomass and the energy required to heat the biomass to the pyrolytic temperature (Elehinafe et al., 2017). Low moisture content is preferable for the synthesis of biochar since it requires less heat energy and less time to complete the pyrolytic process (Asadullah et al., 2008). The variation in ash content among different particle sizes has been attributed to the different friabilities of mineral matter (Yu et al., 2005). The ash content was higher for the smallest particle size. . This result is consistent with findings reported for bagasse, sorghum, Moringa oleifera seed shells, and millet straws (Lori et al.,

2010), indicating high inorganic, volatile, and oxidizable material content. Carbon content helps estimate the char yield from a biomass sample. The presence of oxygen negatively impacts fuel performance; as the oxygen content increases, the heating value decreases (Ryemshak et al., 2016).

Table 2. Characterization results of the Low- and High-density Sawdust

Particle Size (mm)	Sample	M.C %	V.M %	ASH %	F.C %	C %	H %	N %	O %	S %	HHV (MJ/kg)
< 0.6	HDS	8.84	72.45	8.89	9.82	39.22	5.02	1.10	45.11	0.67	18.01
	LDS	8.82	71.04	12.15	7.99	37.41	4.86	1.30	43.59	0.70	17.03
$0.6 \leq x \leq 0.8$	HDS	9.86	81.51	1.21	7.42	41.81	5.34	0.95	50.12	0.58	18.78
	LDS	10.75	78.23	4.19	6.83	39.95	5.14	1.21	48.97	0.54	18.42
$0.8 < x \leq 1$	HDS	9.82	75.89	0.82	13.47	43.11	5.36	0.74	49.39	0.58	20.43
	LDS	9.36	82.16	3.16	5.32	40.77	5.28	1.18	49.04	0.57	17.80

2.2. Experimental Set-up

Response surface methodology (RSM) was employed to identify the most favorable process parameters and address process issues and vulnerabilities. RSM is a cost-effective and precise approach that lowers experimental runs while achieving optimal results. This tool is reliable for developing regression models and analyzing input component interactions (Vinayagam et al., 2022). In this study, major factors (temperature, residence time, and particle size) that contribute to the devolatilization of biomass as reported in the literature were considered. Three levels of temperature (400°C, 450°C and 500°C) and residence time (15, 20, and 25 minutes) together with the particle sizes (<0.6, $0.6 \leq x \leq 0.8$, $0.8 < x \leq 1$ mm) were considered for this study. The study utilized the Central Composite Design (CCD) model, which is a second-order model (Equation 1) incorporating factorial points, axial points, and augmented central points. The model evaluates the substantial impact of each parameter and optimizes the response based on the independent variables. The trials in this investigation were designed using Design-Expert Software Version 8.0.0 (Stat-Ease, Inc., Minneapolis, USA). The experimental design is shown in Table 3. The model competencies were checked with the values of R^2 and adjusted R^2. The authentication of the optimized conditions was done in duplicate to establish the strength of the model.

$$Y = \beta_o + \sum_{i=1}^{k} \beta_i x_i + \sum_{i=1}^{k} \beta_{ii} x_i^2 + \sum_{i=1}^{k} \beta_{ij} x_i x_j + \varepsilon \quad (1)$$

Table 3. Specification of variables and the experimental domain

Variable	Code			
		Experimental Domain		
		-1	0	+1
A	x_1	400	450	500
B	x_2	15	20	25
C	x_3	< 0.6	$0.6 \leq x \leq 0.8$	$0.8 < x \leq 0.1$

A:Teperature, B: Residence time, C: Particle size

The important factors (parameters) that affect the carbonization of biomass are temperature, particle size, and residence time. These parameters were optimized to determine their optimal values for the best product yield and to understand the interaction between these factors. The optimization process was carried out for each of the samples, given their different organic compositions. The fixed carbon, which has a direct relationship with the heating value of the fuel, and the percentage yield are the two responses used for the optimization process. A numerical optimization approach was used to establish the best experimental conditions to achieve the optimal fixed carbon with the corresponding percentage yield. To optimize a system, it is necessary to establish specific objectives for the variables and response. These goals might include achieving a maximum, a minimum, a certain range, or equality. Once these goals are determined, they are integrated into a single desirability function. To identify an optimal combination of conditions that will fulfill all objectives, the three variables were adjusted within a specified range while the response was maximized. The significance of objectives was established as five (5) for fixed carbon and three (3) for percentage yield (Behera et al., 2018).

2.3. Carbonization Process

The carbonization process was carried out using a fixed-bed reactor at Elizade University, Nigeria as shown in Figure 1. The reactor could contain 636.3 cm^3 volume of biomass. It has a cylindrical ceramics band heating element with a power of 1.5 kW making it possible to work at temperatures up to 800°C. A type K thermocouple is attached to the reactor, and connected to a PID controller that senses the temperature of the heating element as the heating progresses. The reactor was designed to be tightly covered to ensure a hermetically sealed reactor to prevent volume and heat loss. The approximate value of the optimal temperatures was input as the PID controller used could not allow decimal numbers. For each experimental run designed, 30g of sample was loaded.

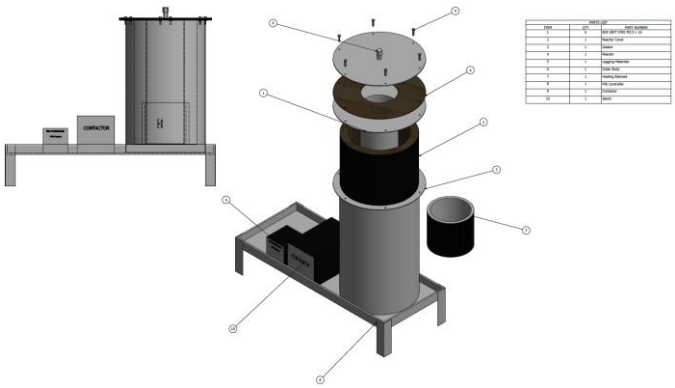

Figure 1: Experimental fixed bed reactor

3. RESULTS AND DISCUSSION

3.1. Optimization and Modelling of Carbonization Parameters

The responses (fixed carbon and percentage yield) of the carbonized HDS and LDS are presented in Table 4. The model's adequacy, based on the acquired data, was assessed for fixed carbon and percentage yield using the sequential model sum of squares. The summary of the analysis of variance (ANOVA) for the selected quadratic model for fixed carbon and percentage yield is shown in Tables 5-8 for the HDS and the LDS. The ANOVA demonstrated that the model is significantly valid, as indicated by the *P* values obtained (P<0.05).

For the fixed carbon of HDS, all model terms (A, B, C, AB, AC, BC, A^2, B^2, and C^2) were significant, each with a *P* value less than 0.0001. For the percentage yield response, only the terms A, B, AB, BC, A^2, B^2, C^2 were significant (*P* <0.05), while the model terms C and AC were not significant (*P* >0.05). In the case of LDS, for fixed carbon, all the terms (A, B, C, AC, A^2, B^2, and C^2) were significant with their respective *P* value less than 0.05, while AB and BC were not significant (P>0.05) and for its percentage yield response, only the terms A and C were significant (*P* <0.05), while the model term B was not significant (*P* >0.05). Lack-of-fit refers to the amount of variance in a model that may be attributed to its insufficiency. The lack of fit was not significant for both models, indicating that the models sufficiently account for the range of responses. Additionally, the predicted and adjusted R^2 values were relatively high, implying that the experimental data can be well explained by the model. The regression models that best describe the process for the fixed carbon and percentage yield of HDS are given in Equations 2 and 3, respectively, while the regression models that best describe the process for the fixed carbon and percentage yield of LDS are given in Equations 4 and 5.

Table 4. Central composite design arrangement and responses for HDS and LDS

SN	A °C	B min	C mm	Fixed Carbon (%) (HDS)	Yield (%) (HDS)	Fixed Carbon (%) (LDS)	Yield (%) (LDS)
1	450	15	$0.6 \leq x \leq 0.8$	49.81	27.91	49.07	31.75
2	500	25	< 0.6	54.75	25.95	47.35	30.23
3	450	20	$0.8 < x \leq 1$	51.35	29.23	50.03	31.70
4	500	20	$0.6 \leq x \leq 0.8$	56.80	25.62	49.63	29.50
5	500	15	$0.8 < x \leq 1$	53.60	27.72	49.80	29.90
6	500	25	$0.8 < x \leq 1$	54.80	25.40	51.12	28.98
7	450	20	$0.6 \leq x \leq 0.8$	52.20	28.30	49.13	31.98
8	450	20	$0.6 \leq x \leq 0.8$	52.25	28.15	49.13	31.86
9	400	25	< 0.6	44.75	32.30	42.93	34.50
10	450	20	$0.6 \leq x \leq 0.8$	52.30	28.10	48.85	31.81
11	450	25	$0.6 \leq x \leq 0.8$	52.62	26.85	51.75	31.77
12	400	20	$0.6 \leq x \leq 0.8$	49.50	31.25	46.30	33.50
13	400	15	$0.8 < x \leq 1$	49.12	32.71	46.78	33.90
14	400	15	< 0.6	40.31	31.85	41.30	34.70
15	450	20	< 0.6	46.80	28.75	44.73	31.80
16	500	15	< 0.6	47.54	26.84	47.75	29.90
17	400	25	$0.8 < x \leq 1$	47.50	32.15	48.79	33.04

A: Temperature, B: Residence time, C: Particle size

$$Y_{\text{Fixed carbon}}\,(\text{HDS}) = 52.23 + 3.63A + 1.41B + 2.22C + 0.696AB - 0.679AC - 1.81BC + 0.9401A^2 - 0.994B^2 - 3.13C^2 \quad (2)$$

$$Y_{\%\text{Yield}}\,(\text{HDS}) = 27.98 - 2.87A - 0.4338B + 0.152C - 0.3875AB - 0.0475AC - 0.305BC + 0.6383A^2 - 0.452B^2 + 1.116C^2 \quad (3)$$

$$Y_{\text{Fixed carbon}}\,(\text{LDS}) = 49.23 + 1.83A + 0.65B + 2.17C + 0.433AB - 0.783AC + 0.10BC - 1.41A^2 + 1.03B^2 - 2.01C^2 \quad (4)$$

$$Y_{\%\text{Yield}}\,(\text{LDS}) = 31.80 - 2.11A - 0.148B - 0.361C \quad (5)$$

Table 5. ANOVA for the quadratic model for HDS using fixed carbon response

Source	Sum of Squares	df	Mean Square	F-value	p-value	
Model	271.66	9	30.18	12400.65	< 0.0001	significant
A-Temperature	131.99	1	131.99	54224.56	< 0.0001	
B-Residence Time	19.77	1	19.77	8121.49	< 0.0001	
C-Particle Size	49.28	1	49.28	20247.49	< 0.0001	
AB	3.88	1	3.88	1593.26	< 0.0001	
AC	3.69	1	3.69	1514.17	< 0.0001	
BC	18.15	1	18.15	7456.75	< 0.0001	
A^2	2.37	1	2.37	974.49	< 0.0001	
B^2	2.65	1	2.65	1087.74	< 0.0001	
C^2	26.32	1	26.32	10811.83	< 0.0001	
Residual	0.0170	7	0.0024			
Lack of Fit	0.0120	5	0.0024	0.9631	0.5804	not significant
Pure Error	0.0050	2	0.0025			
Cor Total	271.67	16				
Predicted R^2 = 0.9997			Adjusted R^2 = 0.9999			

A: Temperature, B: Residence time, C: Particle size

Table 6. ANOVA for the quadratic model for HDS using percentage yield response

Source	Sum of Squares	df	Mean Square	F-value	p-value	
Model	93.99	9	10.44	196.79	< 0.0001	significant
A-Temperature	82.14	1	82.14	1547.79	< 0.0001	
B-Residence Time	1.92	1	1.92	36.15	0.0005	
C-Particle Size	0.2310	1	0.2310	4.35	0.0754	
AB	1.20	1	1.20	22.64	0.0021	
AC	0.0180	1	0.0180	0.3401	0.5781	
BC	0.7442	1	0.7442	14.02	0.0072	
A^2	1.09	1	1.09	20.57	0.0027	
B^2	0.5466	1	0.5466	10.30	0.0149	
C^2	3.59	1	3.59	67.74	< 0.0001	
Residual	0.3715	7	0.0531			
Lack of Fit	0.3498	5	0.0700	6.46	0.1395	not significant
Pure Error	0.0217	2	0.0108			
Cor Total	94.36	16				
Predicted R^2 = 0.9781		Adjusted R^2 = 0.9910				

A: Temperature, B: Residence time, C: Particle size

Table 7. ANOVA for the quadratic model for LDS using fixed carbon response

Source	Sum of Squares	df	Mean Square	F-value	p-value	
Model	117.24	9	13.03	42.68	< 0.0001	Significant
A-Temperature	33.31	1	33.31	109.14	< 0.0001	
B-Residence Time	4.23	1	4.23	13.84	0.0074	
C-Particle Size	47.18	1	47.18	154.59	< 0.0001	
AB	1.50	1	1.50	4.90	0.0624	
AC	4.90	1	4.90	16.05	0.0051	
BC	0.0800	1	0.0800	0.2621	0.6244	
A^2	5.34	1	5.34	17.50	0.0041	
B^2	2.86	1	2.86	9.37	0.0183	
C^2	10.69	1	10.69	35.01	0.0006	
Residual	2.14	7	0.3052			
Lack of Fit	2.09	5	0.4175	17.11	0.0561	not significant
Pure Error	0.0488	2	0.0244			
Cor Total	119.37	16				
Adjusted R^2 = 0.9591		Predicted R^2 = 0.8662				

A: Temperature, B: Residence time, C: Particle size

Table 8. ANOVA for the quadratic model for LDS using percentage yield response

Source	Sum of Squares	df	Mean Square	F-value	p-value	
Model	46.17	3	15.39	144.52	< 0.0001	Significant
A-Temperature	44.65	1	44.65	419.27	< 0.0001	
B-Residence Time	0.2190	1	0.2190	2.06	0.1751	
C-Particle Size	1.30	1	1.30	12.24	0.0039	
Residual	1.38	13	0.1065			
Lack of Fit	1.36	11	0.1234	9.33	0.1007	not significant
Pure Error	0.0265	2	0.0132			
Cor Total	47.55	16				
Adjusted R^2 = 0.9642		Predicted R^2 = 0.9418				

3.2 Interactive Effect of Factors on Fixed Carbon of HDS

The interactive effect of the three factors was examined by plotting 3D graphs, as shown in Figure 2. The curvature of the graphs indicates significant interactions among the factors. In Figure 2(a), the contour shows that as the temperature and residence time increased, the fixed carbon also increased, with the particle size set at $0.6 \leq x \leq 0.8$ mm. Fixed carbon above 50% was observed at temperatures above 450°C and residence times above 20 minutes. The change in the percentage of fixed carbon became insignificant as the residence time increased from 20 to 25 minutes, while it remained significant as the temperature increased from 450 to 500°C. This is within the temperature range observed in the thermal decomposition studies carried out by (Alonge & Obayopo, 2023). The observed rise in fixed carbon content with longer residence time can be attributed to the repolymerization of biomass constituents, allowing sufficient time for their reactions to occur. Conversely, shorter residence times hindered the completion of repolymerization, resulting in a decrease in fixed carbon content (Tripathi et al., 2016). An increase in temperature facilitates the thermal cracking of heavy hydrocarbons, leading to char with high fixed carbon. In Figure 2(b), as the particle size increased from <0.6 mm to $0.6 \leq x \leq 0.8$ mm with an increase in temperature, there was an increase in fixed carbon, while the change in the amount of fixed carbon was insignificant as the particle size changed to $0.8 < x \leq 1$ mm. Fixed carbon above 50% was observed at particle size $0.6 \leq x \leq 0.8$ mm and above, at a temperature greater than 450 °C. Therefore, any particle size less than $0.6 \leq x \leq 0.8$ mm at a temperature less than 450 °C will result in fixed carbon less than 50%. Increasing the particle size increases the distance between the surface of the biomass and its core which results in retardation in heat flow into the biomass (Tripathi et al., 2016). However, an increase in temperature alongside an increase in particle size results in char with higher fixed carbon content. In Figure 2(c), an increase in both residence time and particle size led to an increase in fixed carbon. This shows that adequate time is required for the carbonization of biomass with high particle size to fully take place and for the formation of char with high fixed carbon.

3.3 Interactive Effect of Factors on Percentage Yield of HDS

The interactive effect of the three factors on percentage yield is shown in Figure 3. In Figure 3(a), the contour shows that as the temperature increased, the yield decreased, with the highest yield observed at 400°C. The effect of residence time on the percentage yield was not well pronounced, as the values observed were in very close range. The reduced output seen at a temperature of 500°C can be attributed to the significant volatilization that occurred at higher temperatures. Raising the temperature facilitates the thermal decomposition of complex hydrocarbon molecules, resulting in higher amounts of liquid and gas products and lower production of solid residue. Similar observations were reported by Castillo et al. (2020) who worked on the optimization of biochar production from municipal solid waste. Conversely, prolonging the time that the biomass spends in the reaction environment promotes the full reformation of its constituent compounds, leading to greater production of solid residue (Ryemshak et al., 2016). This aligns with the observations of Kim et al. (2011), as cited by Tripathi et al. (2016), who noted a slight increase in char yield with increasing residence time during the pyrolysis of poplar wood. In Figure 3(b), particle size $0.6 \leq x \leq 0.8$ mm had the lowest yield at all three levels of temperature compared to other particle sizes. The lowest yield at all particle sizes was observed at 500°C, while particle size $0.8<x\leq1$ mm had the highest yield at 400°C. At lower temperatures, thermal cracking of heavy hydrocarbons is minimal, leading to a high yield of char. Mani et al. (2010) reported an increase in biochar yield with increasing particle size from 0.25 to 0.475 mm by pyrolyzing wheat straw. While most publications indicate a high biochar yield trend with rising particle size, a small number of research studies have shown a decrease in biochar yield with increasing biomass particle size (Tripathi et al., 2016).

In Figure 3 (c), particle size $0.6 \leq x \leq 0.8$ mm had the lowest yield as the residence time decreased, while $0.8 < x \leq 1$ mm had the highest yield followed by particle size < 0.6 mm. This implies that particle size $0.6 \leq x \leq 0.8$ mm had the fastest heat transfer rate compared to the other two particle sizes. The longer the biomass residence time, the more the thermal cracking that takes place, and the lesser the char yield. The same outcome was mentioned by Castillo et al. (2020) and Suman & Gautam, (2017). The optimum values were numerically predicted as follows: temperature of 498.24 °C, residence time of 21.16 min, and particle size of $0.6 \leq x \leq 0.8$ mm. The predicted fixed carbon yield under optimum values was 57.40% and the corresponding percentage yield was 25.54%.

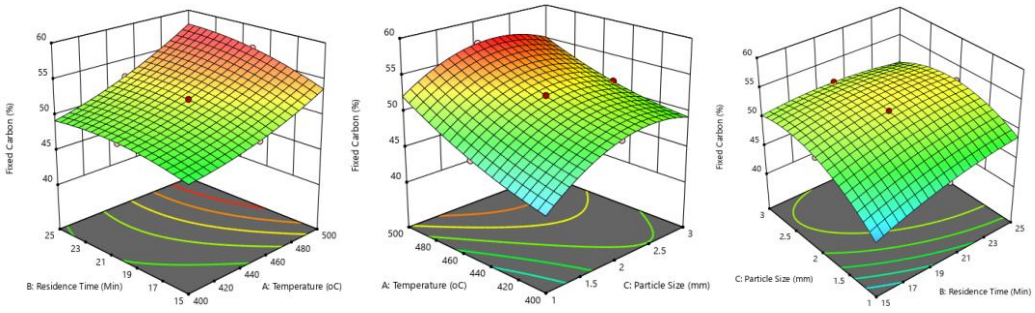

(a) (b) (c)

Figure 2. Contours of the interactive effect of the three factors considered on HDS fixed carbon: (a) residence time against temperature, (b) temperature against particle size, (c) particle size against residence time.

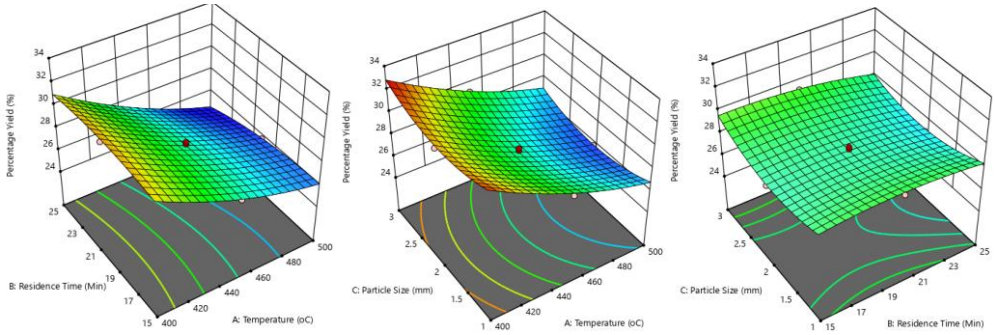

(a) (b) (c)

Figure 3. Contours of the interactive effect of the three factors considered on HDS percentage yield: (a) residence time against temperature, (b) temperature against particle size, (c) particle size against residence time.

3.4 Interactive Effect of Factors on Fixed Carbon of LDS

The interactive effect of the three factors for LDS was examined, as shown in Figure 4. In Figure 4(a), the contour shows that as the temperature and residence time increased, the fixed carbon also increased, while the actual factor was particle size at $0.6 \leq x \leq 0.8$ mm. A similar observation was reported by Liu et al., (2018), who studied the effect of carbonization temperature on the properties of biochar produced from the pyrolysis of crop residues. The fixed carbon content increased at temperatures above 450°C and residence times longer than 23 minutes. The increase in fixed carbon observed with longer residence times during hydrothermal carbonization (HDS) can be attributed to the repolymerization of biomass constituents. This extended reaction time allows for the completion of repolymerization, resulting in higher fixed carbon content. Conversely, shorter residence times do not provide sufficient time for repolymerization to occur, leading to a reduction in fixed carbon content (Cai et al., 2018). A lower amount of fixed carbon was obtained for LDS at different temperatures and residence times compared to HDS. This difference could be due to variations in organic composition and heat transfer rate to the inner core of the biomass. This implies that producing char from HDS will be more economical. In Figure 4(b), as the particle size increased with an increase in temperature, there was an increase in fixed carbon yield. This is consistent with the conclusion reached by Yu et al. (2005). The lowest fixed carbon content was observed at a particle size <0.6 mm and a temperature of 400°C, while the highest fixed carbon content was observed at temperatures above 450°C and particle mm and above. Increasing the particle size increases the distance between the surface of the biomass and its core, resulting in retardation of heat flow into the biomass (Tripathi et al., 2016). Compared to HDS, the rate of char formation was lower for LDS as the particle size increased. This shows that HDS is more effective in char formation than LDS. In Figure 4(c), an increase in both residence time and particle size led to an increase in fixed carbon. The fixed carbon content was low at particle sizes <0.6 mm for all residence times, while the fixed carbon content was higher at a residence time of 25 minutes and particle size $0.6 \leq x \leq 0.8$ mm and above. Sun et al. (2017) reported an increase in fixed carbon as residence time increased. Carbonizing high particle size biomass at low residence times will result in char that is low in fixed carbon. Therefore, to produce char that is rich in fixed carbon, the higher the particle size, the longer the biomass should stay in the reactor

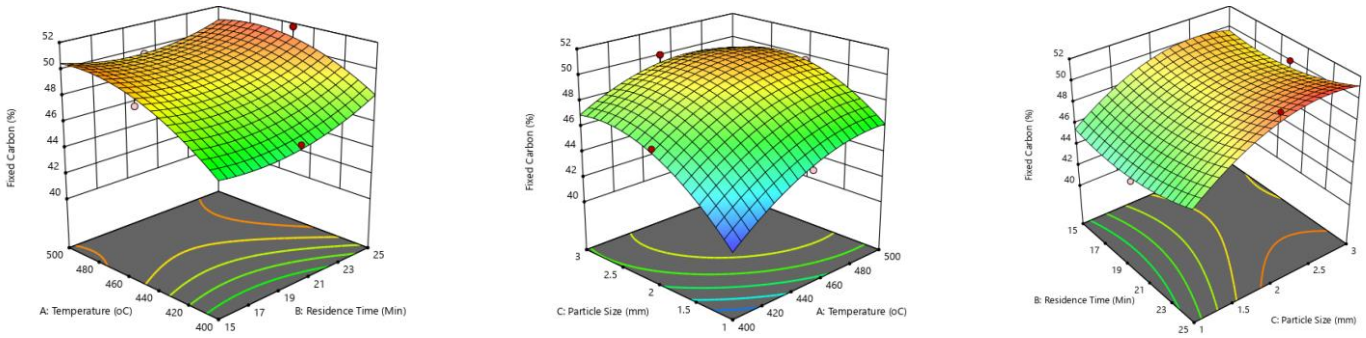

(a) (b) (c)

Figure 4. Contours of the interactive effect of the three factors considered on LDS fixed carbon: (a) residence time against temperature, (b) temperature against particle size, (c) particle size against residence time

3.5 Interactive Effect of Factors on Percentage Yield of LDS

There was no interaction effect between the three factors, as the model was linear. Only the individual factor effect on percentage yield was examined by plotting 2-D line graphs, as shown in Figure 5. The lack of interactive effect indicated that there were no significant interactions among the factors. In Figure 5(a), the line graph shows that as the temperature increased, the percentage yield decreased. In Figure 5(b), it was observed that there was no significant change in percentage yield as the residence time changed. In Figure 5(c), as the particle size increased, the percentage yield decreased. Temperature was the only factor that had a significant effect on the percentage yield, while the effects of particle size and residence time were insignificant. This establishes that temperature is the most important factor of the three considered. A higher percentage yield was recorded for LDS as the temperature increased compared to the percentage yield recorded for HDS. The optimum values for LDS were numerically predicted as a temperature of 474.70 °C, a residence time of 25 minutes, and a particle size of $0.6 \leq x \leq 0.8$ mm. The predicted fixed carbon yield under the optimum values was 51.26%, and the corresponding percentage yield was 30.60%.

3.6 Validation of the Optimized Condition and the Predictive Model

A validation experiment was conducted to confirm the predicted conditions. Table 9 shows that the results aligned with the expected values. The relative error between the anticipated and experimental values for fixed carbon and percentage yield were -2.23% and 8.47%, respectively, for HDS, and -0.63% and 0.62%, respectively, for LDS. This indicates that the model provides a closer prediction for LDS than for HDS.

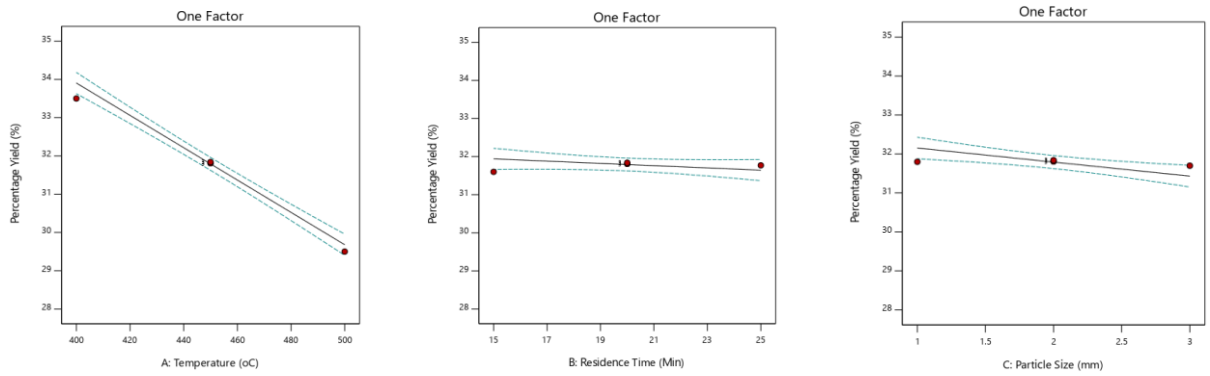

(a) (b) (c)

Figure 5. Contours of the interactive effect of the three factors considered on LDS percentage yield: (a) temperature, (b) residence time, (c) particle size

Table 9. Experimental validation of predicted values in optimal conditions

		Optimal Conditions			$Y_{Predicted}$		$Y_{Experimental}$	
S/N	**Sample**	**Temperature (ºC)**	**Residence Time (min)**	**Particle Size (mm)**	**Predicted Fixed Carbon**	**Predicted % Yield**	**Exp. Fixed Carbon (%)**	**Exp. % Yield**
1	*HDS*	495.49	21.61	0.6 – 0.8	56.86	25.60	55.62 *(-2.23)	27.97 *(8.47)
2	*LDS*	474.7	25	0.6 – 0.8	51.26	30.60	50.94 *(-0.63)	30.79 *(0.62)

*Relative error (%) = [(experimental value − predicted value)/experimental value] × 100%.

3.7 Characterization of the Biochar

The biochar obtained under optimal process conditions was characterized using proximate and ultimate analysis, and the results are presented in Table 10. These results were also compared with coal from various countries (Nigeria, China, India, Turkey). No inherent moisture content was recorded for the HDS- and LDS-sawdust biochar because they were evacuated from the fixed-bed reactor immediately after the carbonization process for analysis. Hashan et al. (2013) reported ash content for coal grading: Ash 8% for superior coal, Ash ≥ 8% < 12% for good coal, Ash ≥ 12% < 16% for fair coal, and Ash > 16% for poor coal. The HDS biochar falls within the range of superior coal, while the LDS biochar falls within the range of good coal. It was observed that the produced sawdust biochar has lower ash content compared to coal. This indicates that the ash present in the produced biochar will not reduce machine efficiency or pose threats to health and the environment. The recorded fixed carbon content was higher than that of coal, whereas the carbon values were lower for coal. The biochar produced exhibited higher oxygen content compared to reported coals, owing to biomass being predominantly composed of cellulose, hemicellulose, and lignin which contain high organic oxygen. In contrast, coal is primarily composed of carbon, hydrogen, nitrogen, and other elements but has a lower oxygen content . The carbonization process enhanced the high heating values (HHV), and the HHV of the sawdust biochar falls within the range of coal from Western China, Owukpa, and Alabama ABD, except for high-ash Indian coal with an HHV of 12.54 MJ/kg. The HHV of coals used in power plants has been estimated to range between 9.5 and 27 MJ/kg (Zactruba, 2009). This suggests that the biochar will be suitable for power generation.

Table 10. Characterization of LDS and HDS biochar

Properties	**HDS-Biochar (Present Study)**	**LDS-Biochar (Present Study)**	**Owukpa Coal (Chukwu et al., 2016)**	**Western Chinese Coal (Ye et al., 2021)**	**High Ash Indian Coal (Kumar & Kumar Nandi, 2021)**	**Alabama-ABD Coal (Bilen, 2019)**
I. M (%)	-	-	11.5	7.55	3.56	-
VM (%)	36.39	37.97	39.1	25.12	18.71	20.59
AC (%)	3.00	11.08	3.3	20.94	57.99	6.61
FC (%)	60.61	50.95	46.1	46.39	19.74	72.80
C (%)	56.26	51.73	67.82	61.14	26.11	84.16
H (%)	4.79	4.39	5.88	3.18	2.26	4.42
N (%)	0.98	1.16	1.43	1.23	1.03	1.48
O (%)	34.50	31.07	9.47	12.95	12.03	2.61
S (%)	0.27	0.34	0.60	0.56	0.58	0.72
HHV (MJ/Kg)	30.00	26.24	26.51	21.93	12.54	33.75

5. CONCLUSIONS

The optimization of process parameters for carbonizing low- and high-density sawdust aimed to identify conditions yielding optimal biochar, potentially substituting fossil fuels. A model was developed to assess temperature, residence time, and particle size's combined impact. Results indicated temperature's predominant influence on fixed carbon and yield, evident from its high coefficient in the model equation. The model accurately predicted optimal conditions, delineated each parameter's significance, and considered their interactions. Enhanced characteristics of both sawdust types (LDS and

HDS), including higher carbon content (56.26% and 51.73%) and energy density (30.0 and 26.24 MJ/kg), were achieved under optimal carbonization conditions. Comparable energy content to coal suggests the biochar as a feasible coal substitute for power generation. Optimal particle size ($0.6 \leq x \leq 0.8$ mm) was recommended for maximizing biochar yield from sawdust. Future studies should evaluate the biochar's performance as a coal alternative further.

6. ACKNOWLEDGEMENT

The authors appreciate the central workshop at University of Elizade, Nigeria for providing all the equipment used for this research.

NOMENCLATURE

ASTM	American Society of Testing and Materials
Greek letters	
β_0	Intercept
β_i	Linear coefficient
β_{ii}	Squared coefficient
β_{ij}	Interaction coefficient
x_i, x_j	Factors

REFERENCES

1. Adeboye, B. S., Adewole, B. Z., Adedoja, A. M., Obayopo, S. O., Asere, A. A., Kayode, O., Idris, M. O., & Okediran, I. K. (2021). Optimization and modeling of process parameters on the yield of enhanced pyrolysis oil during co-pyrolysis of cassava peel with polystyrene. *Environmental Challenges*, *5*, 100347. https://doi.org/10.1016/j.envc.2021.100347.
2. Alonge, O. I., & Obayopo, S. O. (2023). Thermogravimetric analysis of high- and low-density sawdust under nitrogen gas atmosphere. *Energy Sources, Part A: Recovery, Utilization, and Environmental Effects*, *45*(3), 8703–8715. https://doi.org/10.1080/15567036.2023.2232746.
3. Álvarez-Bermúdez, C., Anca-Couce, A., Chapela, S., Scharler, R., Buchmayr, M., Gómez, M. Á., & Porteiro, J. (2023). Validation of a biomass conversion mechanism by Eulerian modelling of a fixed-bed system under low primary air conditions. *Renewable Energy*, *215*, 119003. https://doi.org/10.1016/j.renene.2023.119003.
4. Archer, S. A., & Steinberger-Wilckens, R. (2018). Systematic analysis of biomass derived fuels for fuel cells. *International Journal of Hydrogen Energy*, *43*(52), 23178–23192. https://doi.org/10.1016/j.ijhydene.2018.10.161.
5. Asadullah, M., Anisur Rahman, M., Mohsin Ali, M., Abdul Motin, M., Borhanus Sultan, M., Robiul Alam, M., & Sahedur Rahman, M. (2008). Jute stick pyrolysis for bio-oil production in fluidized bed reactor. *Bioresource Technology*, *99*(1), 44–50. https://doi.org/10.1016/j.biortech.2006.12.002.
6. Behera, S. K., Meena, H., Chakraborty, S., & Meikap, B. C. (2018). Application of response surface methodology (RSM) for optimization of leaching parameters for ash reduction from low-grade coal. *International Journal of Mining Science and Technology*, *28*(4), 621–629. https://doi.org/10.1016/j.ijmst.2018.04.014.
7. Bilen, M. (2019). Proximate and Ultimate Analysis Before and After Physical & Chemical Demineralization. *IOP Conference Series: Earth and Environmental Science*, *362*(1), 012092. https://doi.org/10.1088/1755-1315/362/1/012092.
8. Cai, Y., Tay, K., Zheng, Z., Yang, W., Wang, H., Zeng, G., Li, Z., Keng Boon, S., & Subbaiah, P. (2018). Modeling of ash formation and deposition processes in coal and biomass fired boilers: A comprehensive review. *Applied Energy*, *230*, 1447–1544. https://doi.org/10.1016/j.apenergy.2018.08.084.
9. Castillo, K. J. T., Maguyon-Detras, M. C., Migo, V. P., & Alfafara, C. G. (2020). Parametric and optimization studies for biochar production from municipal solid wastes (MSW) via pyrolysis. *012078*, *778*. https://doi.org/doi:10.1088/1757-899X/778/1/012078.
10. Chukwu, M., Folayan, C. O., Pam, G. Y., & Obada, D. O. (2016). Characterization of Some Nigerian Coals for Power Generation. *Journal of Combustion*, *2016*, 1–11. https://doi.org/10.1155/2016/9728278.
11. Debdoubi, A., Amarti, A. E., & Colacio, E. (2005). Production of fuel briquettes from esparto partially pyrolyzed. *Energy Conversion and Management*, *46*(11–12), 1877–1884. https://doi.org/10.1016/j.enconman.2004.09.005.
12. Elehinafe, F. B., Okedere, O. B., Fakinle, B. S., & Sonibare, J. A. (2017). Assessment of sawdust of different wood species in Southwestern Nigeria as source of energy. *Energy Sources, Part A: Recovery, Utilization, and Environmental Effects*, *39*(18), 1901–1905. https://doi.org/10.1080/15567036.2017.1384869.
13. Gnanasekaran, L., Priya, A. K., Thanigaivel, S., Hoang, T. K. A., & Soto-Moscoso, M. (2023). The conversion of biomass to fuels via cutting-edge technologies: Explorations from natural utilization systems. *Fuel*, *331*, 125668. https://doi.org/10.1016/j.fuel.2022.125668.
14. González, O. M., Velín, A., García, A., Arroyo, C. R., Barrigas, H. L., Vizuete, K., & Debut, A. (2020). Representative Hardwood and Softwood Green Tissue-Microstructure Transitions per Age Group and Their Inherent Relationships with Physical–Mechanical Properties and Potential Applications. *Forests*, *11*(5), 569. https://doi.org/10.3390/f11050569.
15. Hashan, M., Howladar, M. F., Jahan, L. N., & Deb, P. K. (2013). *Ash Content and Its Relevance with the Coal Grade and Environment in Bangladesh*. *4*(4). https://www.researchgate.net/publication/236590642
16. Holechek, J. L., Geli, H. M. E., Sawalhah, M. N., & Valdez, R. (2022). A Global Assessment: Can Renewable Energy Replace Fossil Fuels by 2050? *Sustainability*, *14*(8), 4792. https://doi.org/10.3390/su14084792.
17. *https://www.theworldcounts.com/.*
18. Kim, K. H., Eom, I. Y., Lee, S. M., Choi, D., Yeo, H., Choi, I. G., & Choi, J. W. (2011). *Investigation of physicochemical properties of biooils produced from yellow poplar wood (Liriodendron tulipifera) at various temperatures and residence times*. *92*(1), 2–9. https://doi.org/10.1016/j.jaap.2011.04.002.
19. Kumar, P., & Kumar Nandi, B. (2021). Combustion characteristics of high ash Indian coal, wheat straw, wheat husk and their blends. *Materials Science for Energy Technologies*, *4*, 274–281. https://doi.org/10.1016/j.mset.2021.08.001.
20. Lehmann, J., & Joseph, S. (2015). *Biochar for environmental management: Science and technology* (2nd ed.). https://www.taylorfrancis.com/chapters/edit/10.4324/9780203762264-1/biochar-environmental-management-introduction-johannes-lehmann-stephen-joseph
21. Li, T. Y., Xiang, H., Yang, Y., Wang, J., & Yildiz, G. (2021). Prediction of char production from slow pyrolysis of lignocellulosic biomass using multiple nonlinear regression and artificial neural network. *Journal of Analytical and Applied Pyrolysis*, *159*, 105286. https://doi.org/10.1016/j.jaap.2021.105286.
22. Liu, Z., Niu, W., Chu, W., Zhou, T., & Niu, Z. (2018). *Effect of the carbonization temperature on the properties of biochar produced from the pyrolysis of crop residues*. *13*(2), 3429–3446. https://doi.org/10.15376/biores.13.2.3429-3446.
23. Lori, J. A., Myina, O. M., Ekanem, E. J., & Lawal, A. O. (2010). *Preliminary Evaluation of Moringa Oleifera Seed Shells as Precursor for Activated Carbon*. *4*(12). https://www.researchgate.net/publication/214101048.
24. Mani, T., Muragan, P., Abedi, J., & Mahinpey, N. (2010). *Pyrolysis of wheat straw in a thermogravimetric analyzer: Effect of particle size and heating rate on devolatilization and estimation of global kinetics*. *88*, 952–958. https://doi.org/10.1016/j.cherd.2010.02.008.
25. Osamah, M. G. (2006). *Comparison study between hardwood and softwood*. *3*(23). https://iasj.net/iasj/pdf/7bc2080e9043a4bd.
26. Rentizelas, A. A., Tolis, A., & Tatsiopoulos, I. P. (2009). Logistics issues of biomass: the storage problem and multi-biomass supply chain, *13*(4), 887–894. https://doi: 10.1016/j.rser.2008.01.003.
27. Rominiyi, O. L., Adaramola, B. A., Ikumapayi, O. M., Oginni, O. T., & Akinola, S. A. (2017). Potential Utilization of Sawdust in Energy, Manufacturing and Agricultural Industry; Waste to Wealth. *World Journal of Engineering and Technology*, *05*(03), 526–539. https://doi.org/10.4236/wjet.2017.53045.

28. Ryemshak, S. A., Jauro, Al., Putshaka, J. D., & Sori, R. M. (2016). *Ultimate Analysis of some Nigerian coal: Ranking and Suitable Application*. *3*(10). https://www.ijeas.org/download_data/IJEAS0310002.pdf.

29. Suman, S., & Gautam, S. (2017). *Effect of pyrolysis time and temperature on the characterization of biochars derived from biomass*. *39*(9), 933–940. https://doi.org/10.1080/15567036.2016.1276650

30. Sun, J., He, F., Pan, Y., & Zhang, Z. (2017). *Effects of pyrolysis temperature and residence time on physicochemicalproperties of different biochar types. Acta Agriculturae Scandinavica, Section B—Soil & Plant Science*. *67*(1), 12–22. http://dx.doi.org/10.1080/09064710.2016.1214745

31. Tripathi, M., Sahu, J. N., & Ganesan, P. (2016). Effect of process parameters on production of biochar from biomass waste through pyrolysis: A review. *Renewable and Sustainable Energy Reviews*, *55*, 467–481. https://doi.org/10.1016/j.rser.2015.10.122.

32. Vinayagam, R., Dave, N., Varadavenkatesan, T., Rajamohan, N., Sillanpää, M., Nadda, A. K., Govarthanan, M., & Selvaraj, R. (2022). Artificial neural network and statistical modelling of biosorptive removal of hexavalent chromium using macroalgal spent biomass. *Chemosphere*, *296*, 133965. https://doi.org/10.1016/j.chemosphere.2022.133965.

33. Yang, Z., Wu, Y., Zhang, Z., Li, H., Li, X., Egorov, R. I., Strizhak, P. A., & Gao, X. (2019). Recent advances in co-thermochemical conversions of biomass with fossil fuels focusing on the synergistic effects. *Renewable and Sustainable Energy Reviews*, *103*, 384–398. https://doi.org/10.1016/j.rser.2018.12.047.

34. Ye, C., Ye, Z., Zhu, Z., & Wang, Q. (2021). Thermodynamic and Economic Analysis of Oxy-Fuel-Integrated Coal Partial Gasification Combined Cycle. *ACS Omega*, *6*(6), 4262–4272. https://doi.org/10.1021/acsomega.0c05277.

35. Yu, D., Xu, M., Sui, J., Liu, X., Yu, Y., & Cao, Q. (2005). Effect of coal particle size on the proximate composition and combustion properties. *Thermochimica Acta*, *439*(1–2), 103–109. https://doi.org/10.1016/j.tca.2005.09.005.

36. Zactruba, J. (2009). *Burning coals in power plants- calorific value and moisture*. http://www.brighthu-bengineering.com/power-plants/22202-burning-coal-in-power-plants-calorific-value-and-moisture.

37. Zhao, J., Liu, C., Hou, T., Lei, Z., Yuan, T., Shimizu, K., & Zhang, Z. (2022). Conversion of biomass waste to solid fuel via hydrothermal co-carbonization of distillers grains and sewage sludge. *Bioresource Technology*, *345*, 126545. https://doi.org/10.1016/j.biortech.2021.126545.

38. Zhou, Y., Remón, J., Pang, X., Jiang, Z., Liu, H., & Ding, W. (2023). Hydrothermal conversion of biomass to fuels, chemicals and materials: A review holistically connecting product properties and marketable applications. *Science of The Total Environment*, *886*, 163920. https://doi.org/10.1016/j.scitotenv.2023.163920.